Three-dimensional cathodoluminescence characterization of a semipolar GaInN based LED sample

Matthias Hocker, Pascal Maier, Ingo Tischer, Tobias Meisch, Marian Caliebe, Ferdinand Scholz, Manuel Mundszinger, Ute Kaiser, and Klaus Thonke

Citation: J. Appl. Phys. **121**, 075702 (2017); doi: 10.1063/1.4976204
View online: http://dx.doi.org/10.1063/1.4976204
View Table of Contents: http://aip.scitation.org/toc/jap/121/7
Published by the American Institute of Physics

Three-dimensional cathodoluminescence characterization of a semipolar GaInN based LED sample

Matthias Hocker,[1,a)] Pascal Maier,[1] Ingo Tischer,[1,b)] Tobias Meisch,[2] Marian Caliebe,[2] Ferdinand Scholz,[2] Manuel Mundszinger,[3] Ute Kaiser,[3] and Klaus Thonke[1]
[1]*Institute of Quantum Matter/Semiconductor Physics Group, University of Ulm, Albert-Einstein-Allee 45, 89081 Ulm, Germany*
[2]*Institute of Optoelectronics, University of Ulm, Albert-Einstein-Allee 45, 89081 Ulm, Germany*
[3]*Electron Microscopy Group of Materials Science, University of Ulm, Albert-Einstein-Allee 11, 89081 Ulm, Germany*

(Received 26 October 2016; accepted 18 January 2017; published online 15 February 2017)

A semipolar GaInN based light-emitting diode (LED) sample is investigated by three-dimensionally resolved cathodoluminescence (CL) mapping. Similar to conventional depth-resolved CL spectroscopy (DRCLS), the spatial resolution perpendicular to the sample surface is obtained by calibration of the CL data with Monte-Carlo-simulations (MCSs) of the primary electron beam scattering. In addition to conventional MCSs, we take into account semiconductor-specific processes like exciton diffusion and the influence of the band gap energy. With this method, the structure of the LED sample under investigation can be analyzed without additional sample preparation, like cleaving of cross sections. The measurement yields the thickness of the p-type GaN layer, the vertical position of the quantum wells, and a defect analysis of the underlying n-type GaN, including the determination of the free charge carrier density. The layer arrangement reconstructed from the DRCLS data is in good agreement with the nominal parameters defined by the growth conditions. *Published by AIP Publishing*. [http://dx.doi.org/10.1063/1.4976204]

I. INTRODUCTION

Scanning electron microscope cathodoluminescence (SEM-CL) is a powerful tool to investigate semiconductor materials.[1,2] SEM-CL provides a high lateral resolution of the recorded luminescence patterns due to the active positioning of the primary electron (PE) beam, resulting in a well-defined position of the excitation. For GaN, a typical lateral resolution of ≈50 nm can be obtained for low primary electron energies.[3] To extend the spatial resolution of the SEM-CL spectroscopy into the third dimension, the size and shape of the resulting excitation volume have to be known.[4] This information about the excitation volume for depth-resolved cathodoluminescence spectroscopy (DRCLS) is obtained by Monte-Carlo-simulations (MCSs) of the PE scattering in the semiconductor material. From the simulation of the PE scattering, the locally deposited energy and hereby the intensity of the resulting expected CL can be calculated using established MCS tools like CASINO.[5] Of course, not only simple layers buried in the bulk material but also three dimensional structures can be investigated by DRCLS, as reported, e.g., by Bano *et al.*[6] However, most simulations neglect semiconductor-specific material properties such as the band gap energy or the sample-specific exciton diffusion length, which might have a major impact on the spatial resolution and especially on the depth resolution.[7] We use well established models for the modeling of the PE scattering and extend the resulting energy deposition depth profile by taking into account both exciton diffusion and local variation of band gap energies. Furthermore, we record SEM-CL maps of basal plane stacking faults (BSFs) deeply hidden in the bulk semiconductor material, resulting in a semi-3D map of the luminescence characteristics. Finally, a detailed three-dimensional schematic of the sample under investigation is reconstructed from the data obtained by DRCLS measurements. All values determined by DRCLS are compared to the nominal values expected from growth conditions and high-resolution SEM images and are found to be in good agreement.

II. SIMULATION OF THE EXCITATION VOLUME

The depth resolution used in our study is modeled by a self-written code for MCSs of the PE scattering. The algorithm of the simulation is depicted in Fig. 1: The simulation starts at the sample surface with a single PE at a defined energy E_0. Then, the scattering cross section σ_M^T is calculated. The analytical, semi-empirical approximation of the Mott scattering cross section published by Gauvin and Drouin[8,9] reads

$$\sigma_M^T = 5.21 \times 10^{-21} \frac{Z^2}{E^2} \frac{4\pi\lambda}{\alpha(\alpha+1)} \left(1 - e^{-\beta\sqrt{E}}\right) \left[\frac{E+511}{E+1022}\right]^2, \quad (1)$$

where λ and β are material constants. E is the actual electron energy in keV, and Z is the atomic number. The required individual values for Ga, In, and N can be found in Table I. α denotes a screening factor[10]

[a)]Author to whom correspondence should be addressed. Electronic mail: matthias.hocker@uni-ulm.de
[b)]Present address: Richter Lighting Technologies GmbH, Böbinger Strasse 34, 73540 Heubach, Germany.

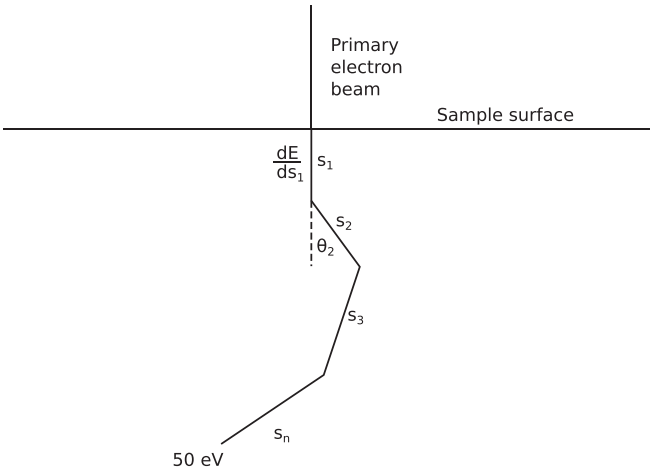

FIG. 1. Schematics of the simulation algorithm.

$$\alpha = 3.4 \times 10^{-3} \frac{Z^{2/3}}{E}. \tag{2}$$

β and λ can be calculated using Eqs. (3) and (4)[8,9]

$$\beta = \frac{26.42}{Z^{1.42}}, \tag{3}$$

$$\lambda = 1.162 + 1.28 \times 10^{-2} Z. \tag{4}$$

The mean free path Λ of the electron in the solid can be calculated from the cross section calculated in Eq. (1) by the expression[12]

$$\frac{1}{\Lambda} = \frac{\varrho N_A \sigma_M^T}{A}, \tag{5}$$

where N_A is Avogadro's constant and A the mass number. For the density of mass ϱ, a value of 6150 kg/m^3 was used for GaN[13] and 6810 kg/m^3 for InN, respectively.[14] The values for InGaN were calculated by linear interpolation. The final length of the n-th path element s_n (see also Fig. 1) reads[15]

$$s_n = -\lambda \ln(R), \tag{6}$$

where R is a random number between 0 and 1. Following the so-called continuous slowing down approximation (CSDA), the electron is considered to loose its energy continuously along the path between two scattering events. Zhenyu and Yancai suggested an empiric formula based on the equations of Joy and Luo[16,17]

$$\frac{dE}{ds} = -\frac{\varrho Z}{JA} \frac{10^4}{0.303(E/J)^{-1/2} + 1.16(E/J)^{1/2} + 0.147(E/J)}, \tag{7}$$

TABLE I. Material parameters.[11]

	Mass number	Atomic number
Ga	69.72	31
In	114.82	49
N	14.007	7

where E is the actual electron energy in eV, s is the length of the path (in nm) over which the electron looses its energy (compare Fig. 1), and J is the mean ionization potential, which can be written as[18]

$$\begin{aligned} J &= 9.76Z + 58.5Z^{-0.19} && \text{for } Z \geq 13 \\ J &= 11.5Z && \text{for } Z \leq 12. \end{aligned} \tag{8}$$

For compound materials, J,Z, and A can be replaced by

$$\begin{aligned} \bar{J} &= \exp\left(\sum_i (C_i Z_i/A_i)\right) \ln J_i / \sum_i (C_i Z_i/A_i)) \\ \bar{Z} &= \sum_i (C_i Z_i/A_i) / \sum_i (C_i/A_i) \\ \bar{A} &= 1/\sum_i (C_i/A_i). \end{aligned} \tag{9}$$

Here, i denotes the i-th element in the compound and C_i the corresponding atomic fraction. Subsequently, the polar scattering angle Θ can be calculated from the partial elastic Mott cross-section[19]

$$\cos(\Theta^{\beta^*}) = 1 - \frac{2\alpha^* R}{1 + \alpha^* - R}. \tag{10}$$

R is again a random number equally distributed between 0 and 1. α^* and β^* are material parameters, which are functions of the actual electron energy. They can be calculated by[19]

$$\begin{aligned} \log_{10}(\alpha^*) &= a_1 + b_1 \log_{10}(E) + c_1 \log_{10}(E)^2 \\ &\quad + \frac{d_1}{\exp(\log_{10}(E))}, \\ \beta^* &= a_2 + b_2 * \sqrt{E} \ln(E) + \frac{c_2 \ln(E)}{E} + \frac{d_2}{E}. \end{aligned} \tag{11}$$

The parameters a-d are given in the tables in Ref. 19. The azimuthal scattering angle is assumed to be homogeneously distributed over 2π. For the simulation in compound semiconductor materials, we introduce another random number that decides which element is hit by the PE in the next scattering event. Here, the probability of hitting a specific atom type is proportional to its atomic fraction. The simulation algorithm is repeated, until the energy of the PE drops below 50 eV. This scattering simulation is repeated for 30,000 electrons. During this MCS, the energy loss of the PEs is recorded at every position inside the excitation volume. By integration over the x-y-plane (i.e., the planes parallel to the sample surface), a depth profile of the deposited energy can be calculated. Now, the relative number of created excitons for each depth can be calculated using the assumption that the creation of each exciton requires three times the band gap energy of the actual semiconductor material.[20] Subsequently, the axial diffusion (i.e., parallel to the incident electron beam) is also taken into account by convolving the exciton creation depth profile with a Gaussian, which decays to $1/e$ over the exciton diffusion length L. The result is a depth profile of the expected CL intensity including the semiconductor-specific material parameters like band gap

energy and diffusion length. The comparison of these MCSs to the intensity of spectral features in the DRCLS spectra allows us to determine the depth in the sample, where a specific CL signal is generated.

III. SAMPLE DESCRIPTION

The light-emitting diode (LED) sample under investigation was grown on a pre-structured *r*-plane sapphire substrate by metalorganic vapor phase epitaxy (MOVPE). First, trenches with a period of 6 μm parallel to the sapphire's *a*-direction were prepared by reactive ion etching using photo-resist as an etch mask. This etching creates tilted side facets with one side facet oriented close to the *c*-plane. On these *c*-plane like side facets, a thin AlN:O nucleation layer was deposited. Afterwards, a GaN buffer layer was grown at 1080 °C by MOVPE for 3.5 min. Then, the temperature was slowly ramped down to 1000 °C and a submonolayer of SiN_x was deposited for defect reduction.[21] The GaN stripes emerging from the trenches finally coalesce to a closed $(11\bar{2}2)$ surface. After coalescence, the growth temperature was set to 970 °C. Subsequently, 2 μm of silicon-doped GaN were grown with a charge carrier concentration of approximately $1 \times 10^{19}\,\mathrm{cm}^{-3}$. On top of the n-type GaN, 5 InGaN quantum wells (QWs) were grown with a thickness of 2.2 nm and a nominal indium content of about 30%. The nominally undoped intermediate GaN barriers have a thickness of 6.5 nm. The QWs were capped with a 40 nm thick layer of undoped GaN, followed by 100 nm magnesium-doped p-type GaN with a free charge carrier concentration of about $p = 4 \times 10^{17}\,\mathrm{cm}^{-3}$. Finally, a 10 nm thick heavily p-doped GaN:Mg layer was deposited to improve ohmic contacts.

IV. EXPERIMENTAL

All CL measurements were carried out in a hot field emitter type scanning electron microscope (SEM) Zeiss LEO DSM 982. A liquid helium-cooled cryostat allows sample temperatures between 7 K and 475 K. The SEM is equipped with an UV-enhanced glass fiber, which collects about 15% of the luminescence light emitted by the samples. The advantages of this method are a low working distance (less than 5 mm), a fully functional inlens detector system, and the possibility of measurements with very low primary energies down to 500 eV. Spectra are recorded by an open-electrode charge coupled device (CCD) with a quantum efficiency of about 0.3 in the relevant spectral region, attached to a 90 cm focal length monochromator. In the configuration used for the measurements presented here, a $300\,\mathrm{mm}^{-1}$ grating blazed for 500 nm was used. The spectral resolution was set to 11 meV at 3.5 eV emission energy. A pivoted mirror can redirect the luminescence light to a smaller 25 cm focal length monochromator equipped with a photomultiplier tube in order to record wavelength-selective CL maps. The resolution of the latter monochromator was set to 29 meV at 3.5 eV, with a $1200\,\mathrm{mm}^{-1}$ grating blazed for 500 nm, as well. The CL measurements were carried out at approximately 8 K, the PE energy was varied in 1 keV steps between 2 and 12 keV, with a sample current between 40 (at 2 keV) and 70 pA (at 12 keV). The resulting not constant excitation power also enters the simulation parameters. For reference purposes, a cross section was prepared by focused ion beam (FIB). For the FIB preparation and high-resolution SEM (HRSEM) investigation, a Zeiss NVision 40 Ar was used.

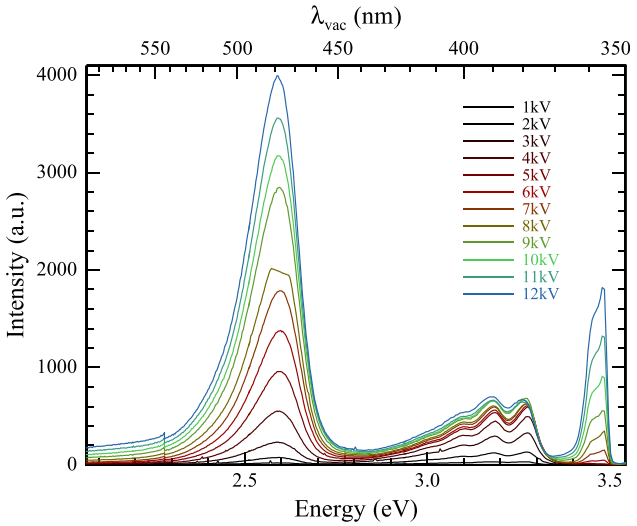

FIG. 2. CL spectra at various PE energies. The donor-bound excitonic and stacking fault related emission bands (>3.4 eV) appear for PE energies above 6 keV.

V. RESULTS

Fig. 2 shows low temperature CL spectra recorded at various PE energies on the surface of the sample described above. The luminescence bands of the QW (2.2–2.8 eV), p-GaN (2.8–3.35 eV), and n-GaN (3.35–3.55 eV) were integrated individually. The corresponding Fig. 3 contains these integrated luminescence intensities as a function of the maximum excitation depth determined by the MCS. Each point represents the integrated luminescence intensity of one of the three features at a specific electron beam energy. For low energies, the spectrum in Fig. 2 is dominated by the features

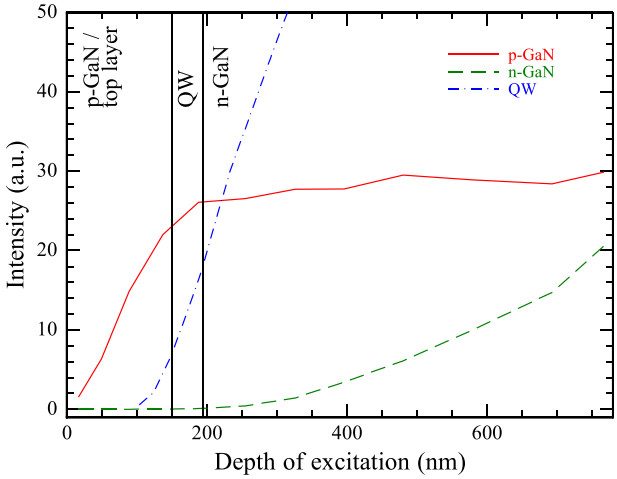

FIG. 3. Measured CL luminescence intensity profile as a function of the depth. The depth values were calculated from the MCS for each PE energy. The vertical lines denote the nominal layer borders as expected from the growth parameters.

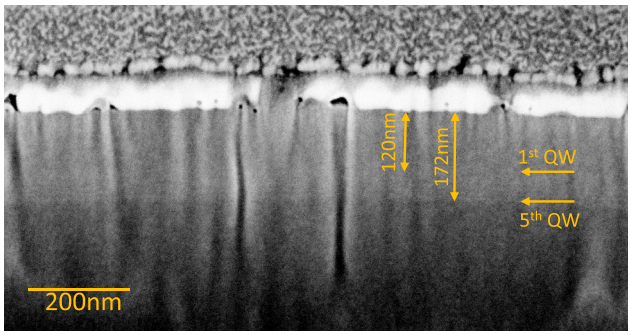

FIG. 4. HRSEM image on the FIB-prepared cross section. At the surface of the sample, metal was deposited to protect the surface during preparation. The QWs are visible as a weak contrast in the inlens-detector image as horizontal lines (see arrows).

between 2.80 and 3.35 eV, which can be assigned to p-type GaN, e.g., donor-acceptor-pair-transitions and their phonon replicas.[22–24] At a calculated penetration depth of 150 nm, the slope of the p-GaN luminescence intensity profile (red solid line) in Fig. 3 decays and finally saturates, because no additional p-GaN is excited with increasing PE energy anymore. This result agrees perfectly with the nominal value. Fig. 4 shows the HRSEM image of the FIB-prepared cross section. The bright contrast on the top are metal layers, which were deposited to protect the surface during the milling process. The image was taken by an inlens detector and the QWs are visible as horizontal lines. The horizontal arrows point to the first and last QWs, which are displayed as weak contrasts. The distance from the surface to the first QW was found to be 120 nm and the distance to the lowest QW was 172 nm. Hence, the QW stack seems to be located 30 nm higher than expected from the growth conditions. Additionally, the lower interface of the pGaN can be identified by the point where the luminescence of the next layer, i.e., the QW, set in. We find that for 2 keV the QW-related emission between 2.2 and 2.8 eV sets in. Some exemplary profiles of the expected CL intensity for various primary energies calculated with the MCS model described in Section II assuming an axial diffusion length for the excitons of 70 nm in semipolar p-type GaN[25] are shown in Fig. 5. From the profile for 2 keV primary energy (solid blue line),

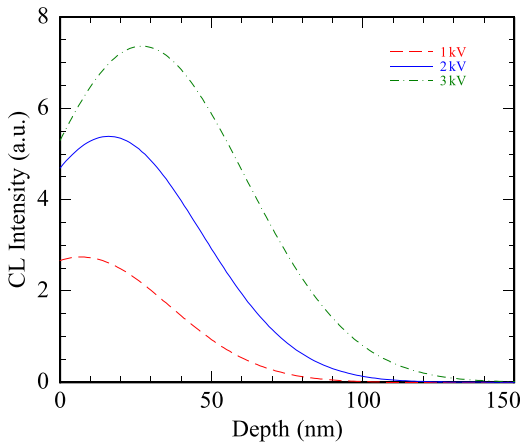

FIG. 5. CL intensity depth profile in GaN calculated by MCS assuming an axial diffusion length of 70 nm for various energies.

the maximum depth, which can be reached by the diffusing excitons created by the 2 keV PE beam, can be determined. This profile reaches a maximal depth of approximately 120 nm when including exciton diffusion, while for depths above 120 nm the calculated CL intensity is zero. That means the DRCLS yields a depth of 120 nm below the sample surface for the upper border of the QW stack, because the luminescence of the QW set in at 2 keV PE energy and the corresponding penetration depth of 120 nm, which agrees perfectly with the value determined by HRSEM. This value can also be seen in the profile of the QW luminescence intensity (dashed and dotted blue line) in Fig. 3, where the QW luminescence sets in. Actually, this penetration depth equals the depth of the QW stack below surface of our LED type sample, which corresponds within experimental error to the nominal overall thickness of 150 nm of the top p-doped layers above the QWs and agrees with the value calculated from the saturating p-GaN signal. The QW luminescence itself has a broad low energy shoulder, which might be a result of potential fluctuations in the QW.[26] Hence, the QW luminescence band in the spectrum was fitted by two Gaussian functions (not shown here). Both the full width at half maximum (FWHM) and the center of the two Gaussians are more or less constant for all spectra. The main peak has a FWHM of 120 meV and the shoulder of 270 meV. The two Gaussians are centered around 2.59 and 2.53 eV, respectively. Assuming the 2.2 nm from Section III, the corresponding In content[27] is 35%, which is a little bit larger than expected.

Starting from 6 keV, the emission of the near band edge (NBE) luminescence features (i.e., donor-bound excitons (DBEs) at about 3.48 eV and basal plane stacking faults) contributes to the spectrum between 3.35 and 3.5 eV, which can be assigned to the underlying higher quality n-type GaN. These bandgap-near luminescence features emit at higher energies than the QWs above. Therefore, the exciton diffusion can be neglected in the CL signal depth profile, because the QWs act as efficient capture and recombination centers for the excitons created initially in the top p-GaN layer.[28,29] The corresponding expected CL signal depth profile calculated now without diffusion reaches 185 nm (see also the slope of the green dashed luminescence intensity profile in Fig. 3) at 6 keV, i.e., the DRCLS states, that the n-GaN is located 185 nm below the surface. Actually, the n-GaN underneath the QWs is located nominally at a depth of 194 nm, which again equals the DRCLS results within experimental errorbars. HRSEM yields a value of 172 nm.

The donor-bound exciton emission of the n-GaN is located at 3.48 eV, i.e., slightly blue-shifted relative to the nominal 3.47 eV of donor-bound excitons in unstrained GaN.[30] Here, this emission band has a low-energy shoulder at 3.46 eV and a tail down to 3.35 eV. The contributions between 3.41 and 3.46 eV can be assigned to basal plane stacking faults (BSF) of type I_1 in n-type GaN with varying free charge carrier concentrations in the surrounding material.[31] Nominally, a BSF of I_1 type should emit at 3.41 eV in the unstrained and (nominally) undoped material (see Ref. 32). However in the present case, the BSF-related emission band has also contributions blue-shifted up to 3.46 eV,

while the shift of the donor bound exciton-related band is much smaller, i.e., the energy spacing between the BSF and the DBE is reduced. This can be explained by a high free charge carrier concentration around the BSF, what appears plausible in the present case with the BSF located in the higher doped n-type material.[31] The DBE and BSF luminescence from the n-GaN will be absorbed by the upper layers with lower transition energies (i.e., mainly the p-GaN), but the residual luminescence intensity is still above 22% of the initial value.[33,34] However, for the depth determination of the signal origin, only the penetration depth of the excitation volume for the PE with which the luminescence sets in is relevant. The absolute luminescence intensity can be neglected, as long as it exceeds the lower detection limit.

To achieve lateral resolution and to support the assignments of the different luminescence contributions in the global spectrum recorded on the surface, Fig. 6 shows the spatial distributions of different features as false-color-coded CL maps. These luminescence maps were recorded at 8 keV primary energy for a good signal to noise ratio. Fig. 7 shows the same CL recorded at 2 keV. The maps recorded at other energies are not shown here. The assignment of the different luminescence features to their corresponding depth was done by the interpretation of the data in Figs. 2 and 3, as described above. Fig. 6(a) is a SEM reference image taken at the sample surface from the area under investigation. The parasitically grown particle in the lower left corner was used for position reference purposes only. Fig. 6(b) shows the distribution of the luminescence of the top p-GaN layer including the luminescence energy range from 2.8 to 3.4 eV. Except for some minor fluctuations of the emission energy mainly in the lower third of the image, the luminescence is quite homogeneously distributed, and there is no contribution of

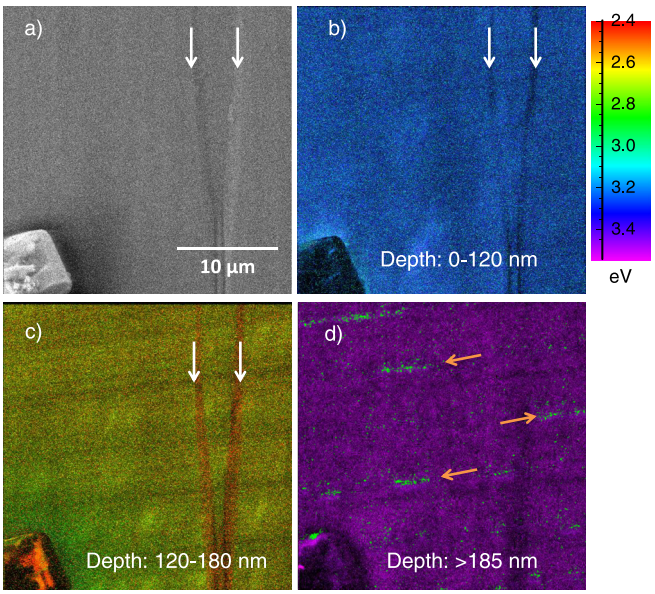

FIG. 6. DRCLS maps. (a) SEM reference image from the surface. The parasitically grown particle in the lower left corner was used for reference purposes; (b) CL map with emission pattern from p-GaN; (c) CL map of the QW-related luminescence; (d) CL map of the NBE emitted from the underlying n-GaN. The light green contrast marks the BSFs, i.e., the luminescence between 3.41 and 3.46 eV (for better contrast, not related to the right color bar).

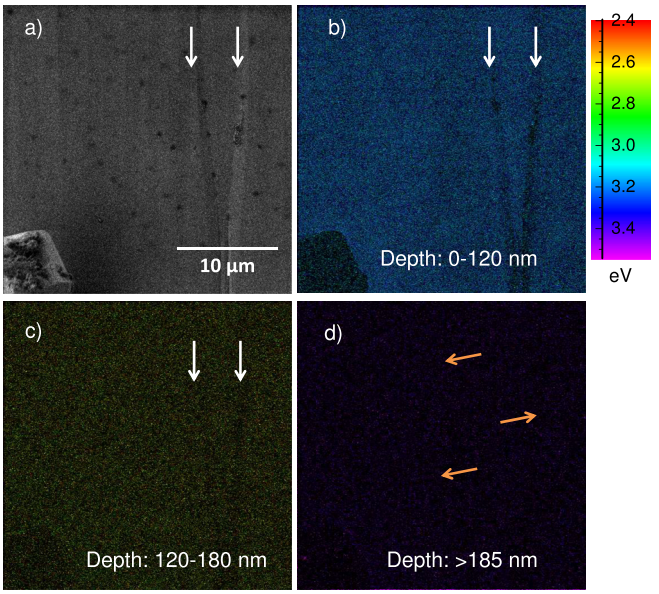

FIG. 7. Reference DRCLS maps, recorded at 2 keV. (a) Reference image; (b) p-GaN layer, the lateral distribution of the luminescence is clearly visible; (c) weak contribution of the QW luminescence; (d) NBE luminescence, nearly no luminescence detected.

stacking faults. The most remarkable feature is caused by the "chevron," which is also visible on the right side of the SEM image (marked by the vertical white arrows). This "chevron" can be observed as a dark contrast in all CL maps correlating with different depths of the sample. It is likely caused by imperfect coalescence of neighboring stripes during the growth procedure of the semipolar sample, causing some kind of step in the coalesced layers.[35] Fig. 6(c) comprises the signal generated mainly in the range between 120 and 180 nm below the surface with photon energies ranging from 2.4 to 2.8 eV. Thus, this map can be assigned to the QWs below the p-GaN, because these luminescence features are not visible for 1 keV PE energy but set in at 2 keV as described above. The QW luminescence shows some dark almost horizontal contrast lines with a spacing of about 6 μm. Obviously, the QW emission brightness reproduces the periodicity of the growth mask. The dark contrasts are caused by bundles of dislocations penetrating the whole sample, including the GaN buffer material, the n-GaN layer, the QWs, and the p-GaN.[36] The borderline of the chevron has a red contrast, which means that most likely more indium is incorporated in the vicinity of structural defects.

Fig. 6(d) finally shows the luminescence distribution of the NBE emission range mainly being emitted from the n-type GaN layer below the QWs. The luminescence is quite homogeneously distributed, only interrupted by the dark contrasts of the dislocations already seen in the QW-related CL map in Fig. 6(c) and the borderline of the chevron in Fig. 6(b). To show the correlation of the CL emission from the deeper layer with I_1 type stacking faults, the BSF emission was superimposed manually using a light green color for the latter (color of this part not correlated with the color bar on the right). These BSFs (marked also by the orange horizontal arrows) can be found exclusively in the vicinity of the dark stripes and reproduce the periodicity of the patterned substrate, as well. Thus,

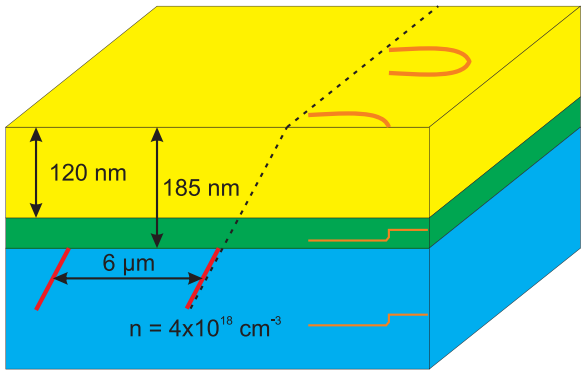

FIG. 8. Reconstructed sample structure from DRCLS measurements. The upper yellow layer denotes the p-type GaN, the middle green one the five-fold Ga(In)N QW, and the lower blue one the n-type GaN. The tilted red lines symbolize the position of the BSFs. The dashed black lines symbolize the dislocation bundles, and the orange contours the chevrons on the surface. The orange line with the kinks symbolizes the imperfect coalescence, which causes steps and results in the chevrons.

the BSFs either penetrate from the early stage growth to the surface or they are created during coalescence. The orientation of these elongated luminescence patterns parallel to the projection of the *c*-plane supports the assignment to BSFs. By comparing the BSF emission energy to numeric simulations,[31] the free charge carrier concentration can be estimated to be $n = 4 \times 10^{18}\,\mathrm{cm}^{-3}$, which is slightly lower than the expected nominal $n = 1 \times 10^{19}\,\mathrm{cm}^{-3}$. Fig. 7 shows the same series of CL maps recorded at 2 keV PE energy. The white arrows mark the borders of the large defect, as in Fig. 6. The luminescence distribution of the p-GaN related signal from the upper sample layers is clearly visible in Fig. 7(b). The QW-related luminescence of the CL map in Fig. 7(c) is very weak, as expected from the spectra series. At least Fig. 7(d) shows the distribution of the NBE luminescence. The inclined orange arrows point to the spots, where the BSFs were found at higher PE energies. This luminescence is very weak; the signal mainly consists of noise and a clear localization cannot be found. The comparison of Figs. 7 and 6 supports the depth assignments, which were discussed above.

Fig. 8 and Table II show the layer arrangement of the LED sample under investigation as reconstructed from the DRCLS measurements discussed above, summarizing the different findings. The values expected from growth conditions and determined by HRSEM are listed in the table, as well. From DRCLS, the upper p-doped GaN (yellow) was found to be 120–150 nm thick. In a depth of 185 nm, the n-doped GaN layer (light blue) starts, and the QWs (green) are located in between. Dislocations (symbolized by dashed black lines) penetrate through all layers of the LED sample up to the surface. Some spots of imperfect coalescence (orange stripes in the bulk n-GaN and QW, "chevron" marked by white arrows in Fig. 6) are also continued in the upper layers, visible as a chevron (orange) on the surface. Inside the n-GaN, BSFs of I_1 type were found (inclined red lines in Fig. 8), allowing to determine the free charge carrier concentration to be $n = 4 \times 10^{18}\,\mathrm{cm}^{-3}$ from their blue shift. The BSF signal roughly reproduces the spatial 6 μm periodicity of the substrate structure. The BSFs might be partially blocked at the interface to the QWs, which can be seen by comparison of Figs. 6(c) and 6(d). Here, the position of the BSFs and the modulation of the QW luminescence pattern do not correlate. The BSFs do not have any impact on the QW luminescence characteristics here.

TABLE II. Comparison of nominal and experimental values. The last line gives the carrier densities in the deeper lying n-GeN layer. The number in braces is the value determined by the saturation of the p-GaN signal.

	Nominal depth	HRSEM	DRCLS result
Top layers (nm)	0–150	0–120	0–120 (150)
QW-Stack (nm)	150–193.5	120–172	120–185
n-GaN (nm)	>193.5	>172	>185
Carrier density	$n = 1 \times 10^{19}\,\mathrm{cm}^{-3}$		$n = 4 \times 10^{18}\,\mathrm{cm}^{-3}$

VI. CONCLUSION

We demonstrated detailed DRCLS investigations on a LED sample grown on semipolar GaN. By simulating the depth distribution of the energy deposition density induced by the primary electrons and also taking into account diffusion of the free excitons generated, the position (i.e., the depth below the surface) of the individual luminescent layers could be determined with high accuracy. Additionally to typical DRCLS measurements, where only the depth of the different features is determined from a series of integral spectra, our measurement allows us to create semi three-dimensionally resolved CL maps. Thus, we could clearly locate the depth and the lateral distribution of the BSFs in the bulk material below the QWs. Furthermore, is was possible to estimate the free charge carrier concentration of the n-type GaN layer. All findings are summarized in the reconstructed model in Fig. 8, demonstrating the amount of data, which can be obtained by DRCLS. All values determined by DRCLS are in good agreement with the nominal properties expected from the growth conditions and determined by HRSEM.

ACKNOWLEDGMENTS

For technical support in the structuring of the template, we thank C. Steinmann and R. Rösch.

[1]A. Gustafsson, M.-E. Pistol, L. Montelius, and L. Samuelson, J. Appl. Phys. **84**, 1715 (1998).
[2]K. Thonke, I. Tischer, M. Hocker, M. Schirra, K. Fujan, M. Wiedenmann, R. Schneider, M. Frey, and M. Feneberg, IOP Conf. Ser.: Mater. Sci. Eng. **55**, 012018 (2014).
[3]C. Donolato, Optik **52**, 19 (1978).
[4]L. J. Brillson, J. Phys. D: Appl. Phys. **45**, 183001 (2012).
[5]D. Drouin, A. Couture, D. Joly, X. Tastet, and V. Aimez, Scanning **29**, 92 (2007).
[6]N. Bano, I. Hussain, O. Nur, M. Willander, Q. Wahab, A. Henry, H. Kwack, and D. L. S. Dang, J. Lumin. **130**, 963 (2010).
[7]C. Donolato, Phys. Status Solidi A **141**, K131 (1994).
[8]R. Gauvin and D. Drouin, Scanning **15**, 140 (1993).
[9]Z. Czyzewski, D. MacCallum, A. Romig, and D. Joy, J. Appl. Phys. **68**, 3066 (1990).
[10]J. Henoc and F. Maurice, in *Use of Monte Carlo Calculations in Electron Probe Microanalysis and Scanning Electron Microscopy*, edited by K. Heinrich, D. Newbury, and H. Yakowitz (U.S. Dept. of Commerce, National Bureau of Standards, 1976), pp. 61–95.
[11]N. Ashcroft, I. Mermin, and N. David, *Solid State Physics*, edited by D. G. Crane (Saunders College Publishing, 1976).

[12]K. Murata, T. Matsukawa, and R. Shimizu, Jpn. J. Appl. Phys., Part 1 **10**, 678 (1971).
[13]V. W. L. Chin, T. L. Tansley, and T. Osotchan, J. Appl. Phys. **75**, 7365 (1994).
[14]T. Tansley, "Crystal structure, mechanical properties, thermal properties and refractive index of InN," in *Properties of Group III Nitrides* (INSPEC, 1993), Chap. 1.5, pp. 36–37.
[15]L. Reimer, *Scanning Electron Microscopy Physics of Image formation and Microanalysis*, Springer Series in Optical Sciences Vol. 45 (Springer, 1998).
[16]T. Zhenyu and H. Yancai, Scanning **24**, 46 (2002).
[17]D. Joy and S. Luo, Scanning **11**, 176 (1989).
[18]M. Berger and B. Seltzer, *Studies in Penetration of Charged Particles in Matter* (National Academy of Sciences-National Research Council, 1964).
[19]D. Drouin, R. Gauvin, and D. Joy, Scanning **16**, 67 (1994).
[20]R. Alig and S. Bloom, Phys. Rev. Lett. **35**, 1522 (1975).
[21]M. Caliebe, T. Meisch, B. Neuschl, S. Bauer, J. Helbing, D. Beck, K. Thonke, M. Klein, D. Heinz, and F. Scholz, Phys. Status Solidi C **11**, 525 (2014).
[22]B. Monemar, P. P. Paskov, G. Pozina, C. Hemmingsson, J. P. Bergman, S. Khromov, V. N. Izyumskaya, V. Avrutin, X. Li, H. Morko, H. Amano, M. Iwaya, and I. Akasaki, J. Appl. Phys. **115**, 053507 (2014).
[23]M. A. Reshchikov, D. O. Demchenko, J. D. McNamara, S. Fernández-Garrido, and R. Calarco, Phys. Rev. B **90**, 035207 (2014).
[24]I. Akasaki, H. Amano, M. Kito, and K. Hiramatsu, J. Lumin. **48–49**(Part 2), 666 (1991).
[25]M. Hocker, P. Maier, L. Jerg, I. Tischer, G. Neusser, C. Kranz, M. Pristovsek, C. Humphreys, D. Heinz, O. Rettig, F. Scholz, and K. Thonke, J. Appl. Phys. **120**, 085703 (2016).
[26]P. Dawson, S. Schulz, R. Oliver, M. Kappers, and C. Humphreys, J. Appl. Phys. **119**, 181505 (2016).
[27]B. Neuschl, J. Helbing, K. Thonke, T. Meisch, J. Wang, and F. Scholz, J. Appl. Phys. **116**, 183507 (2014).
[28]F. Binet, J. Duboz, C. Grattepain, F. Scholz, and J. Off, Mater. Sci. Eng. B **59**, 323 (1999).
[29]P. Blom, C. Smit, J. Haverkort, and J. Wolter, Phys. Rev. B **47**, 2072 (1993).
[30]K. Kornitzer, T. Ebner, K. Thonke, R. Sauer, C. Kirchner, V. Schwegler, M. Kamp, M. Leszczynski, I. Grzegory, and S. Porowski, Phys. Rev. B **60**, 1471 (1999).
[31]M. Hocker, I. Tischer, B. Neuschl, K. Thonke, M. Caliebe, M. Klein, and F. Scholz, J. Appl. Phys. **119**, 185703 (2016).
[32]R. Liu, A. Bell, F. A. Ponce, C. Q. Chen, J. W. Yang, and M. A. Khan, Appl. Phys. Lett. **86**, 021908 (2005).
[33]J. F. Muth, J. H. Lee, I. K. Shmagin, R. M. Kolbas, H. C. Casey, B. P. Keller, U. K. Mishra, and S. P. DenBaars, Appl. Phys. Lett. **71**, 2572 (1997).
[34]O. Ambacher, W. Rieger, P. Ansmann, H. Angerer, T. Moustakas, and M. Stutzmann, Solid State Commun. **97**, 365 (1996).
[35]M. Caliebe, Y. Han, M. Hocker, T. Meisch, C. Humphreys, K. Thonke, and F. Scholz, Phys. Status Solidi B **253**, 46 (2016).
[36]T. Sugahara, H. Sato, M. Hao, Y. Naoi, S. Kurai, S. Tottori, K. Yamashita, K. Nishino, L. T. Romano, and S. Sakai, Jpn. J. Appl. Phys., Part 2 **37**, L398 (1998).